EJNMMI Research

ORIGINAL RESEARCH

Open Access

Non-invasive visualization of pH changes within the tumor-micro-environment by positron emission tomography

Jürgen Brück[1*†], Dominik Schauenburg[2,3†], Seah Ling Kuan[2], Simeon Göttert[1], Benedikt Klasen[1], Veronika Frommberger[1], Kazem Ebadi Jalal[4], Nabil Boui[4], Aaron Kwiatkowski[2], Lisa Schake[4,5], Tobias Bopp[4,5,6,7], Tozka Bohn[4,5,7], Tanja Weil[2], Mathias Schreckenberger[1] and Matthias Miederer[1,8,9]

Abstract

Background Acidic pH values of the tumor microenvironment (TME) have crucial effects on metastatic behavior, host defense, immune regulation and cellular metabolism. Several studies have shown that the acidity of the interstitial space in the TME influences the functions of cancer and stromal cells, particularly regarding immune effects. Changing intratumoral pH might therefore be a potential target for therapy, and pH imaging might guide further developments. We describe radiopharmaceutical probes for positron emission tomography (PET) that exploit the concept of pH-dependent intratumoral hydrolysis of glycosylamine bonds of PET-tracers ([^{18}F]FDG-4-methoxybenzylamine ([^{18}F]FDG-4MBA) and [^{18}F]FDG-benzylamine ([^{18}F]FDG-BA)) to release [^{18}F]FDG as functional moiety with the aim to non-invasively image pH changes.

Results Nuclear magnetic resonance (NMR) spectroscopy demonstrated hydrolysis at pseudo first order and showed pH dependent hydrolysis time, at which 50% of [^{19}F]FDG-4-methoxybenzylamine ([^{19}F]FDG-4MBA) was cleaved, ranging from 3 h at pH 7.4 over 60 min at pH 6.9 to 45 min at pH 6.5. Hydrolysis of [^{18}F]FDG-4MBA in human serum at pH 7,6 was similar to comparable pH without serum (below 10% FDG release after 2 h). The glycosylamines [^{18}F]FDG-BA and [^{18}F]FDG-4MBA were relatively stable in vitro at pH 8.3 with less than 15% FDG release from [^{18}F]FDG-4MBA and less than 10% FDG release from [^{18}F]FDG-BA within 60 min. Hydrolysis at acidic pH led to [^{18}F]FDG release at pH 6.0 of 71% from [^{18}F]FDG-4MBA and 40% from [^{18}F]FDG-BA at 60 min. In *vitro* uptake into B16F10 or MC38 cells was pH dependent in contrast to FDG uptake. In a preclinical model bearing the two different acidic subcutaneous tumors (B16F10 and MC38), pH differences in the acidic TME were better discriminated with [^{18}F]FDG-4MBA than with [^{18}F]FDG-BA. In vivo neutralization of the acidic extracellular tumor pH prevented pH-dependent cleavage of [^{18}F]FDG-4MBA resulting in decrease of PET signal.

[†]Jürgen Brück and Dominik Schauenburg contributed equally to this work.

*Correspondence:
Jürgen Brück
juergen.brueck@unimedizin-mainz.de

Full list of author information is available at the end of the article

Conclusion The determination of pH differences by glycosylamines radiotracers and PET imaging in acidic TME may serve as a novel marker for various questions such as interaction of pH regulation and response to immunotherapies. Notably, even small pH differences in the acidic TME of different tumors, in the same in vivo model, could be discriminated.

Keywords Visualization of pH changes, Radiopharmaceutical, Tumor-micro-environment, Glycosylamine, Hydrolysis

Graphical abstract

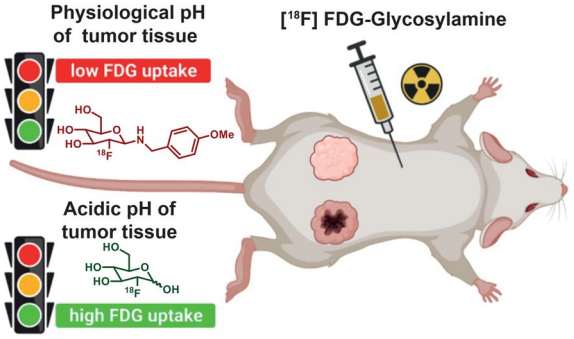

Background

The extracellular acid–base status of most normal tissue in vivo is relatively stable under physiological conditions and close to that of blood. The pH in normal tissues is usually in the range of 7.3 to 7.4, but it varies considerably under certain conditions, as in epithelium (e.g. pancreas, colon, stomach, etc.) during intense acid or base secretion and in skeletal muscle during physical activity. Due to the high metabolic activity and insufficient perfusion of tumors, acidic metabolites often accumulate in tumors and influence the pH of the tumor microenvironment (TME) [1]. It has been shown that the acidity of the interstitial space can influence the functions of cancer and stromal cells and their interaction with the extracellular matrix. Minimal changes in the extracellular pH value in the TME have effects on host defense, metastatic behaviour, immune regulation and cellular metabolism [2, 3]. Changes of the intratumoral pH are spatially and temporally heterogeneous and dependent on numerous factors such as metabolism or cell and vessel density.

Due to the suppression of the immune system e.g. by inhibition of anticancer immune effector cells in acidic pH or the activation of anti-inflammatory M2-like macrophages and regulatory T-cells, elevating the pH in the TME also might serve as a therapeutic target [4, 5]. PET-imaging might provide valuable methods of measuring changes in intratumoral pH. In contrast to approaches such as optical imaging or MRI the use of radiotracers for PET display advantages such as reliable image quantification and feasibility in clinical translation.

In this study we used amine nucleophiles with high pKa values that condense on [^{18}F]FDG and form an acid-labile glycosylamine ([^{18}F]FDG-hemiaminal). This leads to radiotracers that are easy to prepare using commonly available techniques and that exhibits tumor imaging properties under acidic conditions of the TME, when hemiaminal cleavage releases [^{18}F]FDG inside the tumor which then is transported and accumulated into FDG-avid tumor cells [6]. This hemiaminal cleavage is strongly related pH levels in the range found in the extracellular tumor microenvironment.

To validate the method of pH determination by hemiaminal cleavage to free [^{18}F]FDG, we measured uptake from [^{18}F]FDG-4MBA and [^{18}F]FDG-benzylamine in relation to unmodified [^{18}F]FDG uptake in vitro *and in* an in vivo model of two different murine tumor cell lines: 1. the very aggressively growing and strongly acidic melanoma cell line B16F10 (B16) and 2. the colon adeno carcinoma cell line MC38, reflecting a less acidic tumor microenvironment [7, 8].

In contrast to [^{18}F]FDG imaging, where aerobic glycolysis drives [^{18}F]FDG uptake, pH specific imaging with [^{18}F]FDG-4MBA or [^{18}F]FDG-BA depends mainly on the extracellular pH which is responsible for the cleavage of the radiopharmaceutical and only in a second step on FDG uptake by tumor cells.

Methods

Nuclear magnetic resonance (NMR) spectroscopy

The release of [^{19}F]FDG from [^{19}F]FDG-4MBA was monitored using ^{1}H nuclear magnetic resonance (NMR) spectroscopy (Bruker Avance 700 NMR spectrometer). Aromatic protons of the 1,4-substituted ring undergo a significant downfield shift after hemiaminal hydrolysis, and the time courses of release were recorded at different pH values by NMR. Chemical shifts are expressed in parts per million (ppm) and are referenced to residual non-deuterated solvent signals (DMSO). The signals of

[^{19}F]FDG-4MBA and [^{19}F]FDG are well complementary and time of 50% hydrolytic cleavage occurs at the intersection of both curves. 1 mg [^{19}F]FDG-4MBA was dissolved in 500 µL of deuterated phosphate buffer (pH 7.4, 6.9 or 6.5), and 1 mg DMSO (Sigma-Aldrich, Darmstadt, Germany) was added as a reference. Over a period of up to7 hours, a ^{1}H spectrum was recorded every 15 min.

Synthesis of [^{18}F]FDG-4MBA and [^{18}F]FDG-BA

[^{18}F]FDG was obtained from Advanced Accelaration Application, Germany. Synthesis of [^{18}F]FDG-4MBA and [^{18}F]FDG-BA were carried out on a SynChrom R&D module from Elysia Raytest. First, [^{18}F]FDG (500 MBq) was azeotropically dried using 0.5 ml acetonitrile (Riedel-de-Haen, Selze, Germany) under vacuum and a stream of nitrogen. Afterwards, 250 µl of a solution of 0.5 M 4-methoxy-benzylamine or benzylamine (Sigma-Aldrich, Darmstadt, Germany) and 0.25 M acetic acid (Carl-Roth, Karlsruhe, Germany) diluted in water/DMSO (1:1) was added to the dried [^{18}F]FDG. The reaction mixtures were incubated for 30 min at 80 °C under stirring. The reaction mixture was diluted with 4 ml 20% acetonitrile, the crude product was then purified using preparative HPLC on a C18 10 µm column (MZ-Analysentechnik, Mainz, Germany) (isocratic; 15% acetonitrile). The purified fraction was diluted fourfold with HPLC-grade water (Riedel-de-Haen, Seelze, Germany) and concentrated using a C18 Sep Pak Plus cartridge (Waters GmbH, Eschborn, Germany). [^{18}F]FDG-4MBA and [^{18}F]FDG-BA were eluted from the C18 Sep Pak Plus cartridge with 500 µl ethanol (60%; Carl-Roth, Karlsruhe, Germany) and for further in vivo and in vitro experiments diluted with 700 µl sodium hydrogen carbonate buffer (pH 8.4; B. Braun, Melsungen, Germany).

HPLC degradation assay

To initiate pH dependent hydrolysis [^{18}F]FDG-4MBA and [^{18}F]FDG-BA were formulated either with sodium hydrogen carbonate buffer (pH 8.3; B. Braun, Melsungen, Germany), ROTICalipure pH 6.88 and ROTICalipure pH 6.00 (Carl-Roth, Karlsruhe, Germany) and measured three times in an analytical HPLC system at intervals of 30 min.

Serum stability

20 MBq [^{18}F]FDG-4MBA in 250 µl of Aqua ad injectable (B. Braun, Melsungen, Germany) were incubated with 750 µl of human serum or NaCl (control) for 2 h at 37 °C. Afterwards, the serum sample was mixed with 1 mL of acetonitrile and centrifuged at 10,000 rpm for 5 min. The supernatant was filtered through a 0.2 µm syringe filter (Millex-LG, Darmstadt, Germany) and the stability of [^{18}F]FDG-4MBA in human serum versus NaCl was determined using an analytical HPLC system (LiChrosorb RP-18 5 µm (250 × 4 mm) column in an Agilent 1260 infinity HPLC system; 95% water 5% acetonitrile at 0 min to 5% water 95% acetonitrile at 20 min at a flow rate of 1 ml/min).

Cellular tracer uptake study

For in vitro cellular uptake experiments under different pH values in supplemented DMEM pH was adjusted with $NaHCO_3$ or HCl (Carl-Roth, Karlsruhe, Germany). For the basic cell culture media was adjusted to a pH of 7.6, for the neutral cell culture to a pH of 7.0 and for the acidic cell culture to a pH of 6.4 (determined after 24 h at 37 °C in a 5% CO_2 atmosphere). 5×10^6 B16F10 or MC38 tumor cells were suspended in acidic, neutral, and basic media. 0.1 MBq of the radiopharmaceuticals [^{18}F]FDG-4MBA, [^{18}F]FDG-BA or [^{18}F]FDG was added to each sample. Cells were then incubated at 37 °C, 5% CO_2 for 20 min and kept in suspension by shaking once. After washing with PBS 2×10^6 cells were transferred into 3 mL polystyrene tubes (revvity, Hamburg, Germany) and measured via Wizard2 automated γ-counter (Perkin Elmer, Rodgau, Germany) at an energy window of 350 to 650 keV.

Mice

Female C57BL/6JRj mice, were purchased from Janvier. All mice were housed in the animal facility (TARC) of the University Medical Center Mainz. All animal studies were approved by the competent governmental agency Landesuntersuchungsamt Rheinland-Pfalz (G21-1–099) and were performed according to the local regulations. Animals were used at an age of 6–8 weeks and maintained in individually ventilated cages with standard rodent pellet food and water or 200 mM $NaHCO_3$ water (starting 10 days prior tumor cell inoculation). Group sizes were 4–5 animals. The group size for the [^{18}F] glycosylamine distribution in naïve mice compared to [^{18}F] FDG (Fig. 4) were 3 animals.

Tumor cell lines and subcutaneous tumor induction

The B16F10 cell line used is a mouse skin malignant melanoma cell line and MC38 originates from a mouse colon carcinoma (Institute of Immunology University Medical Center, Johannes Gutenberg University Mainz original ATCC). Both were maintained in Dulbecco's modified Eagle's medium (ThermoFisher Scientific, Germany) containing 10% heat-inactivated fetal bovine serum (FBS), 2 mM L-glutamine, 1% penicillin and streptomycin (all from ThermoFisher Scientific, Dreieich, Germany). Tumor cells were taken from the log phase of in vitro growth (70% confluence), cells were trypsinized (Carl Roth, Karlsruhe, Germany), washed in PBS (Sigma-Aldrich, Darmstadt, Germany) resuspended in 0.9% NaCl solution (B. Braun, Melungen, Germany). 100 µL of

tumor-cells were transferred subcutaneously into the left (B16; 2×10^5 cells/mouse) and right (MC38: 1×10^6 cells/mouse) flank of the mice.

Tumor volume was calculated using the following formula: $V = 0{,}5 \times L \times W.^2$

L = longest diameter; W = shortest perpendicular diameter.

PET

For insertion of a venous catheter into the tail vein, tracer injection and subsequent PET measurement, mice were anesthetized with 2% isoflurane evaporated in oxygen at a flow rate of 0.5 L/min (Abbott, Wiesbaden, Germany). After tracer injection the catheter was flushed with 100 µl of saline solution. In total, ~ 5 MBq PET-tracer dissolved in 100 µL 0.9% NaCl solution (B. Braun, Melsungen, Germany) was injected *intravenously.* Whole body PET scans were performed 45 min after injection of [^{18}F]FDG-4MBA, [^{18}F]FDG-BA or [^{18}F]FDG using a dedicated Focus 120 small-animal PET scanner over 12 min under anesthesia on a temperature-controlled bed (Concorde Microsystems/Siemens Preclinical Solutions, Knoxville, USA). PET image reconstruction was performed on a microPET Acquisition Workplace V02.3200 with OSEM3D without scatter or attenuation correction. The reconstructed voxel size was 0.432×0.432x0.796 mm^3. Volumes of interest were drawn manually (PMOD 4.3, Bruker, Ettlingen, Germany) and the percentages of injected dose per cubic centimetre (%ID/cm^3) values were calculated as follows: mean activity in VOI/(injected activity·10^6)/100.

Biodistribution

After the final PET scans, all animals were sacrificed by cervical dislocation under deep anaesthesia, and blood, organs (heart, liver, spleen and kidney) were collected.

After dissection, organ weight was determined, and radioactivity was measured by γ-counting (Wallac 1480 WIZARD 3″ Gamma Counter; PerkinElmer, Waltham, Massachusetts, USA) using an energy window between 350 and 650 keV. For quantification, a standardized aliquot of the injected radiotracer was added to the measurement. The biodistribution results for each organ (B16-tumor, MC38-tumor, heart, liver, spleen, kidney, blood) are expressed as the percentage of the overall injected dose per g (%ID/g).

Ex vivo pH measurement in tumors with unisense microelectrode system

pH-microelectrodes for ex vivo pH measurement of tumors was purchased from Unisense A/S (Aarhus, Denmark). The signals were acquired by a microsensor multimeter (Unisense, Aarhus, Denmark) interfaced with a computer to record data (60–80 subsequent measurements). Tumor-bearing animals were euthanized on day 14 after tumor inoculation, B16 and MC38 tumors were dissected, and the pH was determined directly with the unisense microelectrode system.

Statistics

All data were analyzed and plotted using GraphPad Prism 10 software. Statistical analyses were performed by using two-sided T-tests or the Tukey's post-hoc test after One-way ANOVA as indicated. Values of $P < 0.05$ were considered significant. Descriptive statistics report arithmetic means and standard deviations.

Results

Synthesis of [^{19}F]FDG-4MBA and release of condensed [^{19}F]FDG monitored by ^{1}H nuclear magnetic resonance (NMR)

Hemiaminal-FDG formation using 4-MBA and [^{19}F]FDG under acidic conditions (formic acid) results in [^{19}F]FDG-4MBA, which could be isolated in 66% yield by preparative HPLC (Supplemental Fig. 1).

Under physiological, slightly basic pH (pH 7.4) the decaying time, at which 50% glycosylamine hydrolysis occurs is 3 h (Fig. 1A). Mimicking the pH conditions of a slightly acidic TME (pH 6.9), a shortening to 1 h was found (Fig. 1B). This means that at pH 7.4 two thirds of [^{19}F]FDG are still present at 110 min (the half-life of F-18) as a condensed [^{19}F]FDG complex, whereas at pH 6.9 only one third remains. This is even more pronounced at pH 6.5, where 50% of [^{19}F]FDG is released after 45 min and almost 80% after 110 min (Fig. 1C). Figure 1D shows the stability of the hemiaminals as a function of the pH value. At pH 7.4 there is twice as much bound [^{19}F]FDG as at pH 6.5 after 1 h. After 2 h, this becomes even more significant: At pH 7.4 there is about three times more [^{19}F]FDG hemiaminal compared to pH 6.5.

Synthesis of [^{18}F] glycosylamines and in vitro stability

[^{18}F]FDG-4MBA and [^{18}F]FDG-BA could be eluted at 6–8 min from the preparative C18 column whereas unconjugated free [^{18}F]FDG elutes at 2–4 min (Fig. 2A, B). The average radiochemical conversion, based on integration of HPLC peaks, amounted to 69± 7% at [^{18}F]FDG-4MBA (n = 5) and 64 ± 4% [^{18}F]FDG-BA (n = 4). Preparation and purification of [^{18}F]FDG-4-phenylbenzylamine was not pursued in this study due to the insufficient solubility of 4-phenylbenzylamine and the low product yields.

To confirm the purity of [^{18}F]FDG-4MBA and [^{18}F]FDG-BA for following experiments, both products were injected into an analytical HPLC system. The chromatogram showed high purity (< 90%) of both products (t_R = 8 min) and no free [^{18}F]FDG (Fig. 2C, D). [^{18}F]FDG-4MBA and [^{18}F]FDG-BA were eluted in buffers with increasing acidity and were injected at intervals of 30 min

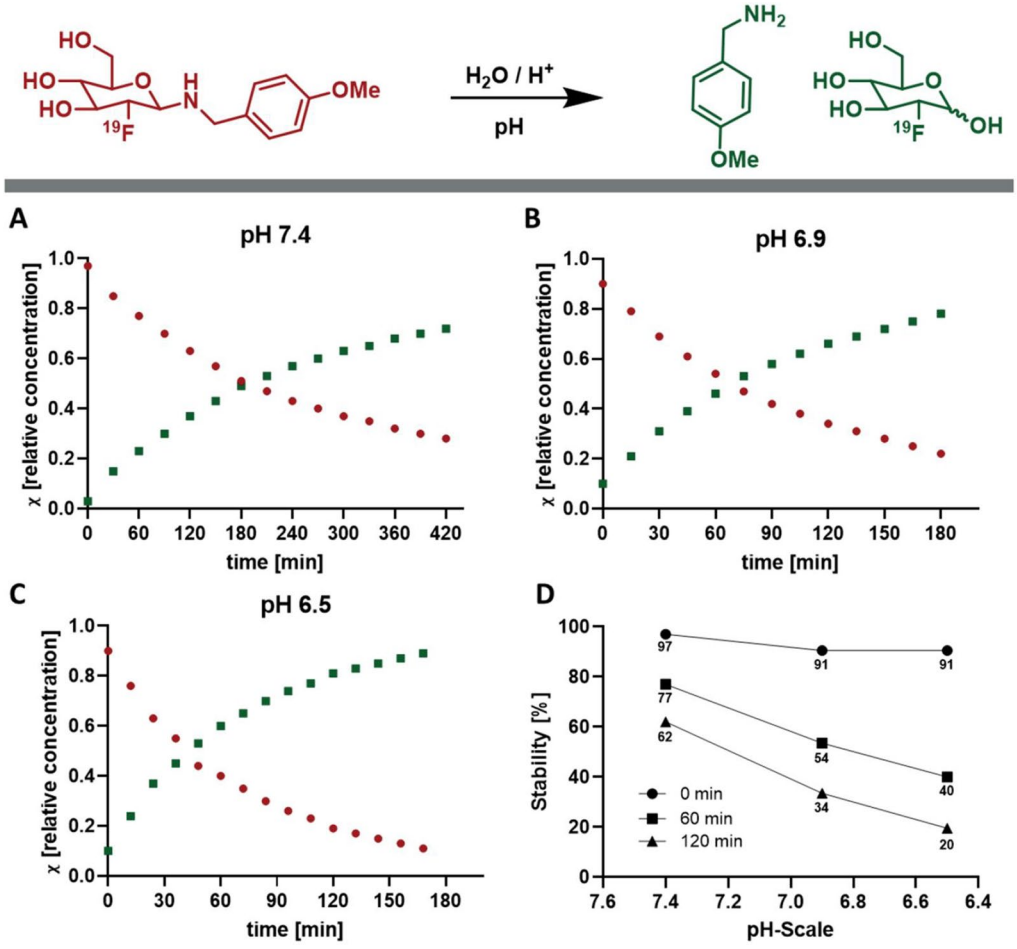

Fig. 1 Hydrolysis of [^{19}F]FDG-4MBA. Time dependent release studies of [^{19}F]FDG-4MBA monitored by 1H nuclear magnetic resonance (NMR) spectroscopy at different pH values

into the analytical HPLC system. [^{18}F]FDG-4MBA and [^{18}F]FDG-BA eluted in a sodium-bicarbonate-buffer (pH 8.3) showed little glycosylamine hydrolysis over more than one hour with FDG release below 15% and 10% (Fig. 2E, F). Hydrolysis of the [^{18}F]FDG-heminaminals at pH 6.00 and pH 6.88 was markedly faster and more pronounced for [^{18}F]FDG-4MBA in comparison to [^{18}F]FDG-BA (Fig. 2G-J).

To investigate the stability of [^{18}F]FDG-4MBA, we quantified as a test for clinical trials, we quantified the stability of [^{18}F]FDG-4MBA in human serum compared to serum-free buffer. Stability assay in 75% human serum at 37 °C demonstrated only little FDG release below 10% over 2 h similar to the FDG release in normal saline (Supplemental Fig. 2).

Tumor cell uptake of [^{18}F] glycosylamines under acidic culture conditions in vitro

Both cell lines showed a pH dependent enrichment of [^{18}F]FDG-4MBA and [^{18}F]FDG-BA (Fig. 3A-D), whereas unmodified [^{18}F]FDG did not show a pH dependent uptake (Fig. 3E, F).

We measured no significant difference in the cellular uptake of [^{18}F]FDG-BA between 6.4 and 7.0 in a pH range corresponding to the TME in vivo (Fig. 3C, D). These data indicate that [^{18}F]FDG-4MBA is similar to the already described [^{18}F]FDG-BA [6] suited to determine pH changes in a range of 7.0 to 7.6 (Fig. 3C, D) and also indicates that the pH optimum for hydrolysis of [^{18}F]FDG-4MBA further extents to even lower pH values.

[^{18}F] glycosylamines distribution in naïve mice compared to [^{18}F]FDG

Uptake in the heart for [^{18}F]FDG was 6.6% ID/g (± 0.87), for [^{18}F]FDG-4MBA 2.1% ID/g (± 0.31) and for [^{18}F]FDG-BA 1,4% ID/g (± 0.13). Uptake into liver was 1,43% ID/g (± 0,87) for [^{18}F]FDG, 1.58% ID/g (± 0.76) for [^{18}F]FDG-4MBA and 1,09% ID/g (± 0.3) for [^{18}F]FDG-BA (Fig. 4).

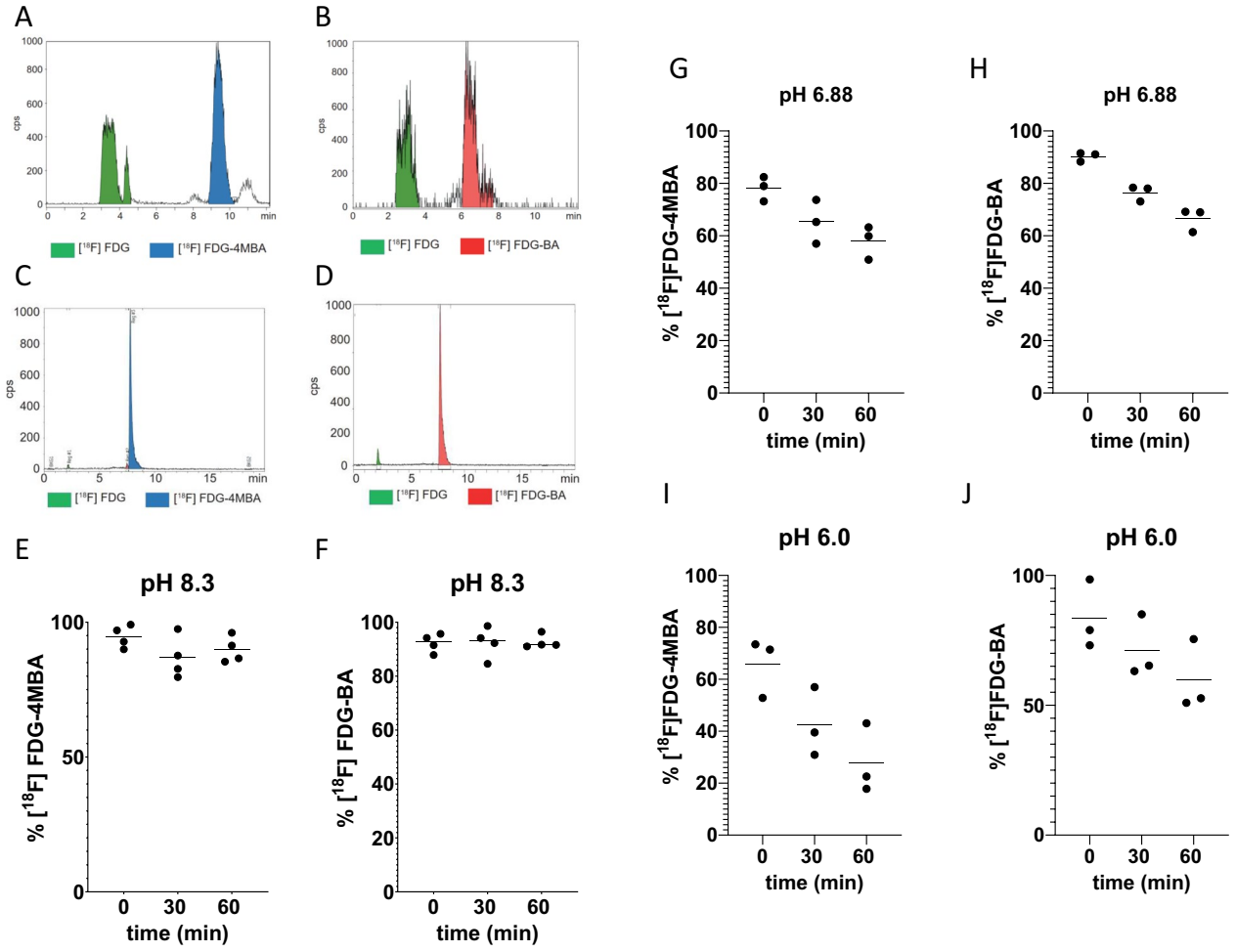

Fig. 2 Synthesis of [^{18}F]FDG-4MBA and [^{18}F]FDG-BA and stability at different pH. Synthesis of [^{18}F]FDG-4MBA and [^{18}F]FDG-BA were carried out in one-step Elysia-Raytest synchron module by incubation of [^{18}F]FDG with 4MBA (**A**) or BA (**B**). The synthesized glycosylamines were purified using a preparative HPLC system. Data show representative analytical chromatograms of [^{18}F]FDG-4MBA and [^{18}F]FDG-BA. (**C** and **D**) pH dependent hydrolysis of [^{18}F]FDG-4MBA and [^{18}F]FDG-BA at pH 8, pH 6.88 and 6.0 and was measured at intervals of 30 min by analytical HPLC (**E**—**J**)

TME pH in the two in vivo *tumor model*

The mean tumor volume of the B16 tumors was 134,6 ± 5,98 mm^3 (n = 4) and the mean tumor volume of the MC38 tumors was 136,3 ± 8,41 mm^3 (n = 4).

B16 tumors had a pH of 6.2 (± 0.32) and MC38 tumors had a pH of 6.7 (± 0.09). In mice fed with alkalized water also intratumoral pH was higher in both B16 melanomas (pH 7.2 ± 0.16) and MC38 adenocarcinomas (pH 7.5 ± 0.11). Unpaired T-Test between both tumors remained significant both for normal and alkalized drinking water (Fig. 5).

PET imaging of tumors with different pH in the TME

[^{18}F]FDG as a marker of glucose metabolism showed no differences in [^{18}F]FDG uptake between B16 (6.61 ± 3.4% ID/cm^3) and MC38 (7.30 ± 1.40% ID/cm^3) in the two tumor model at tumors with similar volumes (B16: 604 mm^3, MC38: 652 mm^3; Fig. 6A, B). Ex vivo biodistribution analysis confirmed the non-invasive in vivo [^{18}F]FDG-PET imaging results, as we determined similar [^{18}F]FDG uptake in B16 (8.7 ± 1.7% ID/g) and MC38 (8.1 ± 1.98% ID/g) tumors, from the same mice (Fig. 6C). Therefore, in line with the in vitro results no major differences between the tumors regarding FDG uptake are present. To investigate whether it is possible to discriminate differences in acidity in the TME we compared [^{18}F]FDG-4MBA and [^{18}F]FDG-BA in the two tumor model. [^{18}F]FDG-4MBA showed a significantly higher uptake in B16 tumors (5.6 ± 1.1% ID/cm^3) compared to MC38 tumors (4.0 ± 0.4% ID/cm^3) (Fig. 6D, E). Again, ex vivo biodistribution analysis confirmed [^{18}F]FDG-4MBA PET imaging results, as we determined a significantly higher [^{18}F]FDG-4MBA uptake in B16 tumors (5.6 ± 0.9% ID/g) compared to MC38 tumors (3,7 ± 0.9% ID/g) (Fig. 6F). In contrast, tumors displayed also uptake of [^{18}F]FDG-BA, but no differences in acidity levels in the TME was shown by [^{18}F]FDG-BA uptake (B16: 4.3 ± 0.8% ID/cm^3 and MC38: 4.4 ± 0.5% ID/cm^3) (Fig. 6G, H). Ex vivo

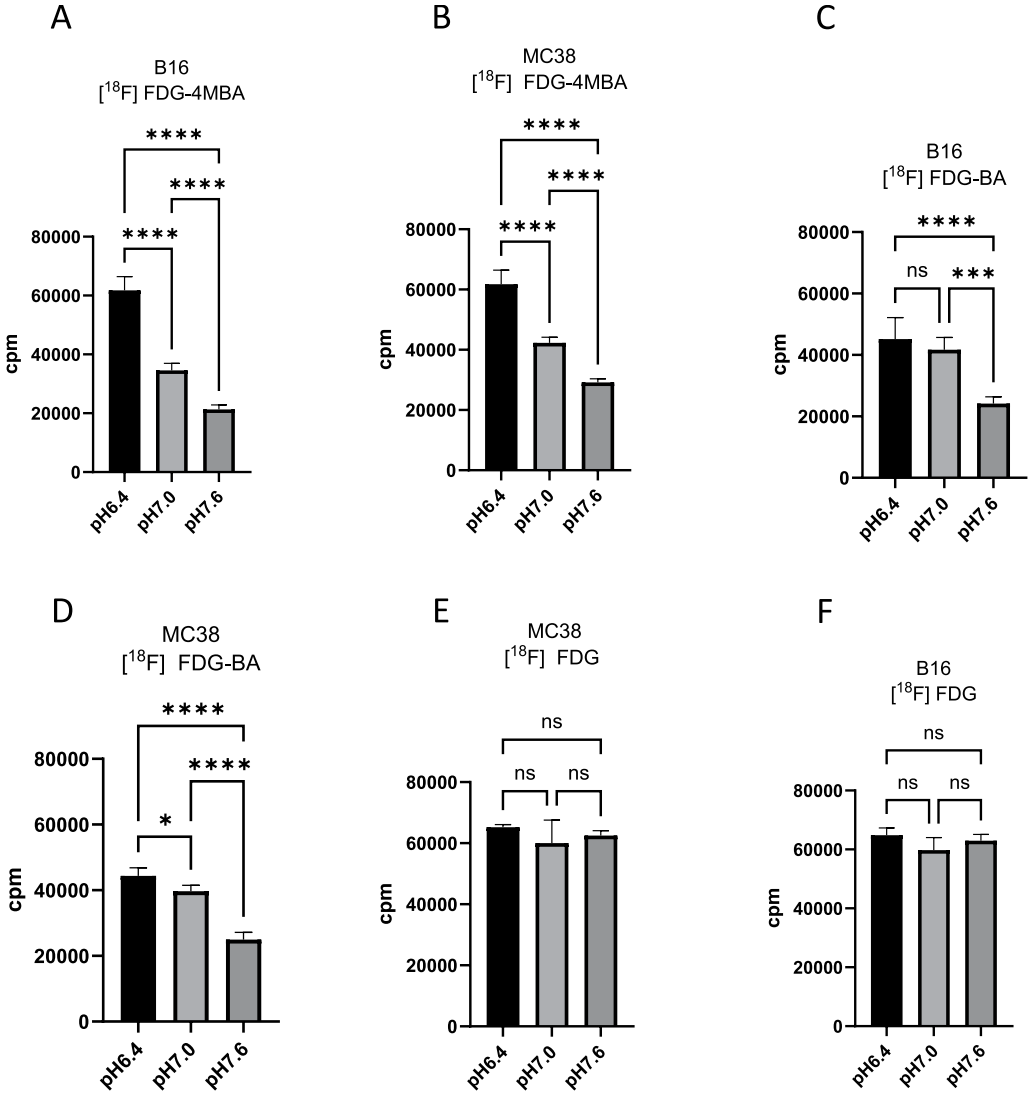

Fig. 3 Cellular uptake of [18F]FDG-4MBA and [18F]FDG-BA under different pH values. (**A**-**F**) tumor cells (B16 and MC38) were cultured under increasing acidity of the cell culture medium from 7.6 to 6.4. Tumor cells were processed with the same level of activity of [18F]FDG-4MBA (**A**-**B**) or [18F]FDG-BA (**C**-**D**) and as a control for a pH independent cellular uptake [18F]FDG (**E**–**F**) was used

biodistribution of tumor-bearing mice after application of [18F]FDG-BA again confirmed the non-invasive imaging data of B16 (4.9 ± 0.76% ID/g) and MC38 (4.7 ± 0.98% ID/g) (Fig. 6I).

[18F]FDG-4MBA uptake after alkalinization of the TME

[18F]FDG-4MBA uptake in B16 tumors from sodium bicarbonate treated mice (2.7 ± 0.7% ID/cm^3) was lower when compared to B16 tumors from non-sodium bicarbonate treated control mice (5.6 ± 1.1% ID/cm^3, Fig. 6E) and was similar to unspecific uptake in the heart (Fig. 7A-C; 6D-F). Ex vivo biodistribution analysis of the experimental mice confirmed the non-invasive in vivo [18F]FDG-4MBA PET imaging results ([18F]FDG-4MBA uptake in sodium bicarbonate-treated mice:2.2 ± 0.5% ID/g; in non-treated animals: 5.64 ± 0.9% ID/g) (Fig. 7C; 6F).

Discussion

Several techniques, many of them based on MR imaging, have been developed for visualizing acidic interstitial pH in vivo [9]. While these techniques have yielded important insights, they are often limited by long scan time, poor spatial resolution, low signal-to-noise, and requirement for administering high doses of probe, potentially altering systemic pH. In contrast, positron emission tomography (PET) has the potential to overcome some of these limitations, owing to its relatively high spatial resolution, ability to inject tracer doses of radiopharmaceuticals, and relative ease of clinical translation. As such, there is a growing interest in PET imaging of

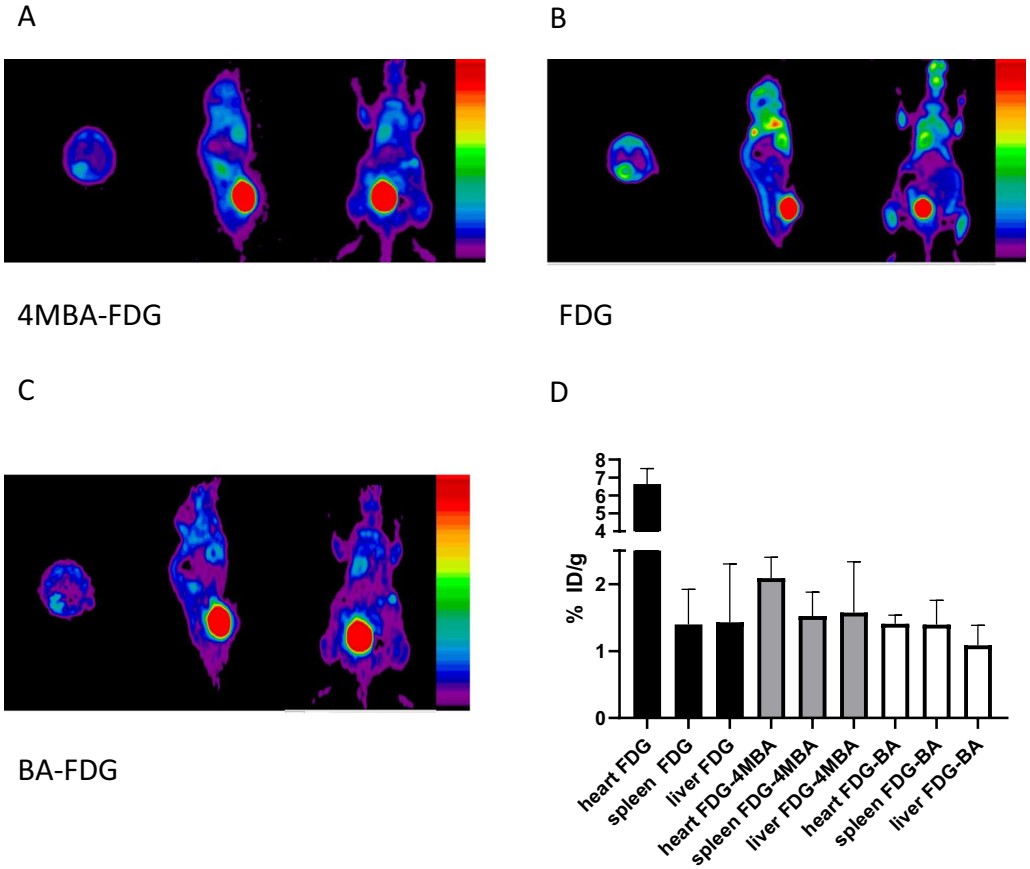

Fig. 4 [^{18}F]FDG-4MBA and [^{18}F]FDG-BA distribution in naïve mice compared to [^{18}F]FDG. [^{18}F]FDG-4MBA, [^{18}F]FDG-BA and [^{18}F]FDG distribution shown by PET 45 min p.i. Images from representative single mice are depicted for [^{18}F]FDG-4MBA (**A**), [18F]FDG-BA (**B**) and [^{18}F]FDG (**C**). Ex vivo biodistribution after PET imaging shows lower uptake to the heart of [^{18}F]FDG-4MBA and [18F]FDG-BA compared to [.^{18}F]FDG and similar liver and spleen uptake (**D**)

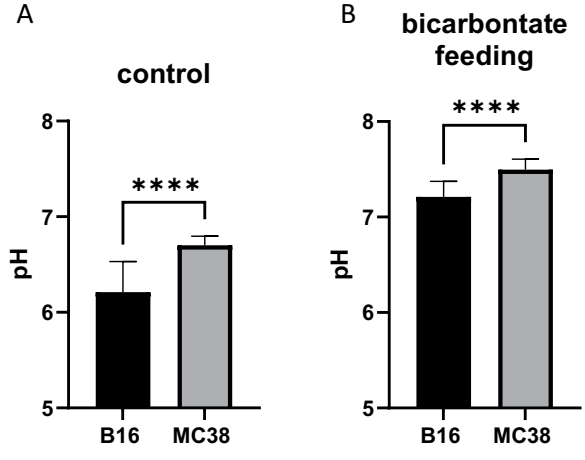

Fig. 5 Tumor microenvironment pH. (**A**) The pH value in the TME of the B16 melanoma (left mouse flank) and the MC38 adenocarcinoma (right flank) on day 14 after tumor cell transfer was determined using a unisense pH electrode system in mice receiving normal drinking water (**A**) or bicarbonate drinking water (**B**)

acidic interstitial pH, and a few examples have been reported, including methods based on charge trapping of labelled radiopharmaceuticals or pH-dependent insertion of engineered peptides into cell membranes [10, 11]. The pH-dependent hydrolysis of glycosylamines has been described and measured for a wide range of glycosylamines more than 70 years ago. In these studies, the authors were also able to show that hydrolysis can be attributed to a limited pH range and display varying pH optima [12, 13]. Flavell et. al. showed that a nucleophilic acid-labile substitution of an amine to [^{18}F]FDG results in an imaging agent for measuring intratumoral pH values [6]. These [^{18}F]FDG hemiaminals function via a two-step mechanism in which the acid-labile [^{18}F]FDG-[nucleophilic substituent] decomposes to form the common radiotracer [^{18}F]FDG, which is subsequently accumulated by glucose-affinity cells. For our study we chose hemiaminals by their pKa with values above 9. Direct comparison of hydrolysis rates is difficult to obtain and might be influenced by numerous factors like e.g. protonation fraction in the respective in vivo conditions and resonance effects of the benzyl. Thus, a systematic

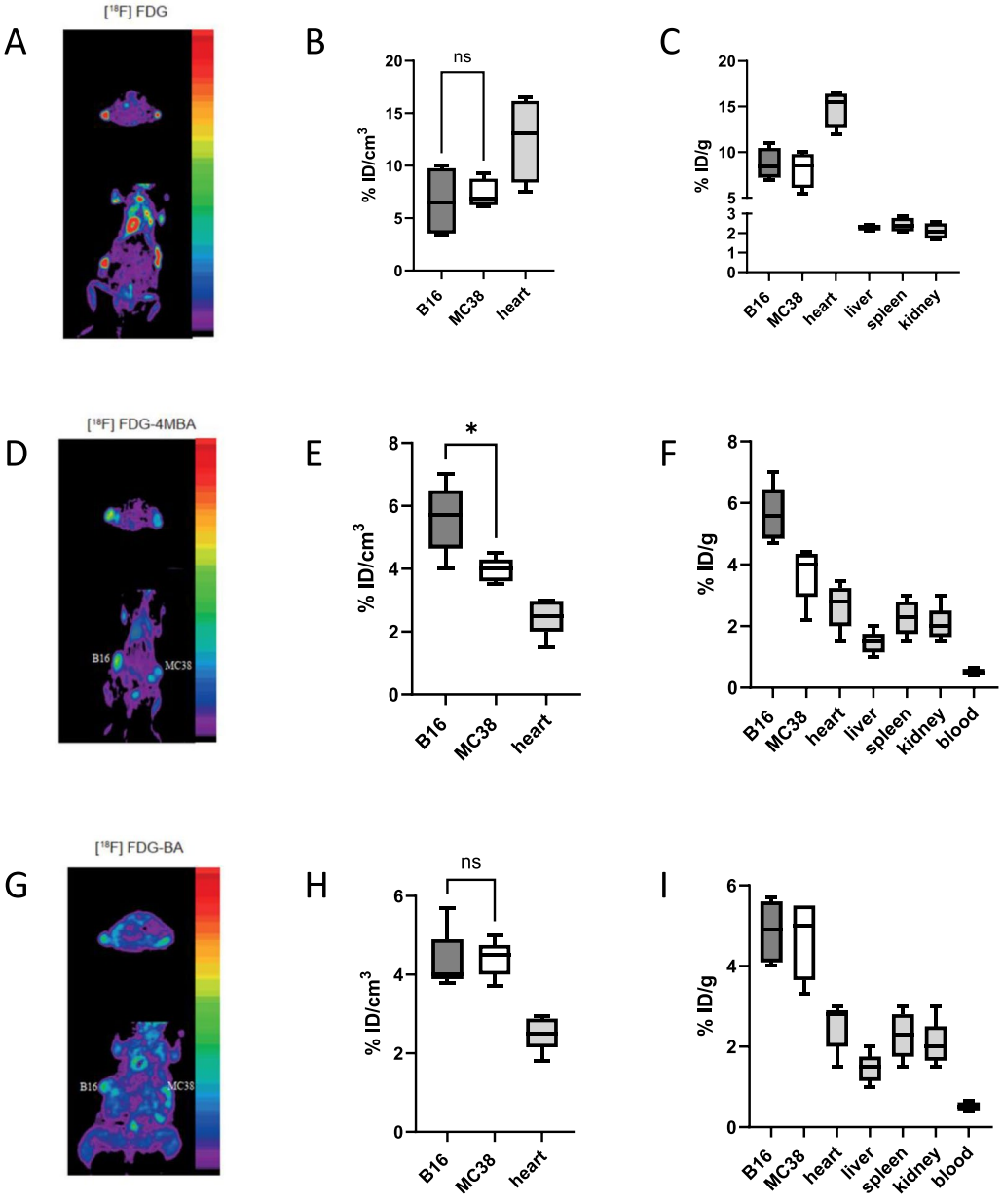

Fig. 6 [^{18}F]FDG, [^{18}F]FDG-4MBA and [^{18}F]FDG-BA PET in tumor bearing mice. Mice received B16 and MC38 tumor cells and imaged on days 12 after tumor cell transfer. [^{18}F]FDG, [^{18}F]FDG-4MBA and [^{18}F]FDG-BA uptake in the TME of B16 and MC38 tumors were quantified by PET imaging and biodistribution. Images from single mice are depicted in (**A**, **D**, **G**). Tumor uptake from [^{18}F]FDG (**B**), [^{18}F]FDG-4MBA (**E**), [^{18}F]FDG-BA (**F**) was measured from volumes of interests manually drawn over tumors and heart and confirmed by biodistribution (**C**,**F**,**I**). Box plots show the median with 25th and 75th interquartile range (IQR) and whiskers indicate 1.5 × IQR. Data in were analyzed using Tukey's post hoc test after One-way ANOVA

in vitro/in vivo evaluation lays the foundation on further development steps. Due to the poor solubility, the difficult synthesis of [^{18}F]FDG-4-phenylbenzylamine ([^{18}F]FDG-4PBA) and the poor yield of this radiopharmaceutical, we decided to use 4-methoxybenzylamine as an amine, which has sterically good properties for fast enough hydrolyzation at slightly acidic pH values. In contrast to 4PBA, 4MBA is more soluble in water and our data obtained in this study show that it is well suited to visualize small pH differences both in vitro and in vivo. In comparison benzylamine is also very soluble in water and the synthesis also provides high yields of [^{18}F]FDG-BA. With the slightly larger substitute the resulting radiotracer [^{18}F]FDG-4MBA showed similarities with [^{18}F]FDG-BA. However, in vitro and in vivo hydrolysis further increased with lower pH values and thus [^{18}F]FDG-4MBA demonstrated better capacity to differentiate the small differences between low acidic MC38 tumors and

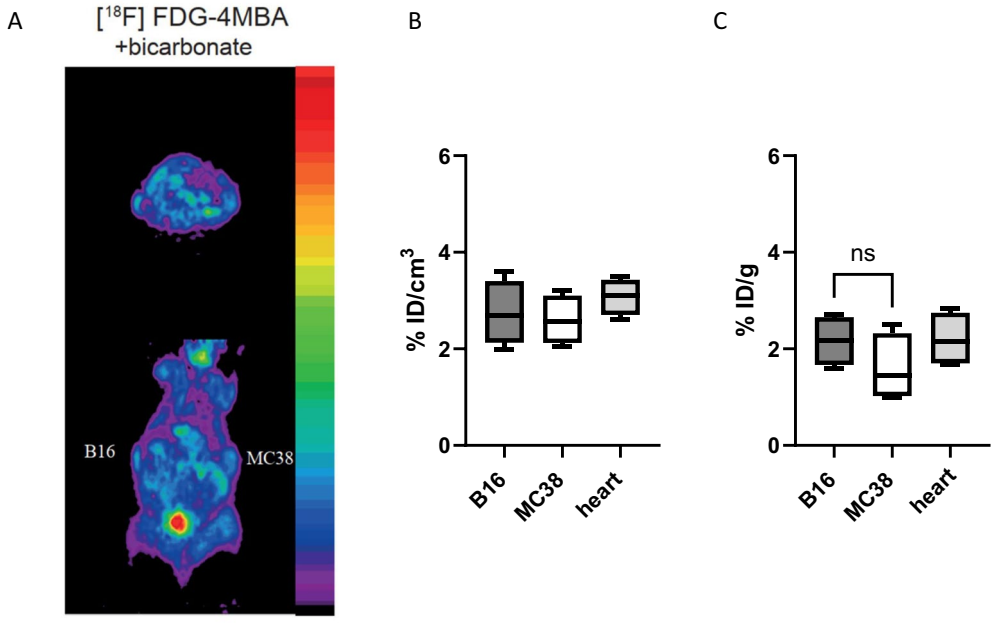

Fig. 7 [^{18}F]FDG-4MBA PET after alkalinization of the TME. Mice received bicarbonate or control water and received B16 and MC38 tumor-cells. Mice were imaged on day 12 after cell transfer. [^{18}F]FDG-4MBA uptake in B16 and MC38 tumors was quantified by PET imaging and biodistribution. Images from a representative mouse are depicted in (**A**). [^{18}F]FDG-4MBA PET analysis (**B**) and biodistribution results (**C**). Box plots show the median with 25th and 75th interquartile range (IQR) and whiskers indicate 1.5 × IQR

high acidic B16 tumors compared to [^{18}F]FDG-BA. In the initial stage of gycosylamine hydrolysis, reversible protonation occurs, wherein the pKa value of the nitrogen plays a crucial role. Ideally, this pKa value should align with the slightly acidic pH of the TME to facilitate protonation, allowing for subsequent cleavage of the radiopharmaceutical into free [^{18}F]FDG and the amine. Nevertheless, since hydrolysis is not only dependent on pK value of the hemiaminal chemical modifications are difficult to predict. Our experiments indicate that a broader pH optimum for [^{18}F]FDG-4MBA exists when compared to [^{18}F]FDG-BA, meaning that this radiopharmaceutical might be more suitable for imaging small pH differences in vivo. Generally, measuring pH values in vivo is associated with many difficulties such as complex and dynamic intra-tumoral processes and a certain level of inhomogeneity in every tumor. Therefore, a clear gold standard of pH measuring cannot be expected. Nevertheless, the consistently measured pH differences in both tumors are reasonable evidence of the reported uptake mechanism. Data have shown that by determining the acidity of the TME, predictions can be made about the aggressiveness of tumor growth, metastatic behavior and the migration and differentiation of immune cells [14, 15]. An alternative option to glycosylamines are small polymers that are degraded under acidic conditions. These are used in new therapeutic approaches to trigger the release of drugs as soon as the drug carrier has reached the slightly acidic tumor environment or after the drug carrier has been taken up by the cells, which leads to the localization of the polymer in the acidic endosomes and lysosomes. The uptake mechanisms of pH sensitive pH tracers vary, for example in regard of the role of tumor cell membrane function. For example, ^{11}C-labeled bicarbonate is hypothesized to be converted to [^{11}C]CO_2 in an acidic environment and then diffuses across the cell membrane [16]. Peptides have been reported to change their conjugation towards alpha helices in acidic environment, that then is inserted into cell membranes [11]. Using Glycosylamines in the form of [^{18}F]FDG-hemiaminal the underlying mechanism of pH imaging is hydrolysis in the tumor environment, and the tumor cell is then accumulating [^{18}F]FDG by an active transport mechanism followed by intracellular trapping. The hydrolysis is a complex reaction where different parameters play a role. We have confirmed the hypothesis that this reaction is well suited to image pH differences. Comparing two slightly different hemiaminals [^{18}F]FDG-4MBA had a broader range of optimal pH compared to [^{18}F]FDG-BA both in vitro and in vivo. However, cardiac uptake of [^{18}F]FDG-4MBA was also higher than for [^{18}F]FDG-BA. This might be explained by an acidic environment also in the mouse heart [17]. Since the pH value of the TME can have a decisive influence on the functionality of immunotherapies, such an imaging method might add a tool to gain mechanistic insight of pH effects during immune therapies.

Conclusion

Glycosylamine based PET tracers display a high potential as pH imaging probes and in particular [^{18}F]FDG-4MBA is a promising tracer to discriminate different acidic tumors.

Supplementary Information

The online version contains supplementary material available at https://doi.org/10.1186/s13550-026-01383-2.

Additional file 1.

Acknowledgements
We thank D. Kerner, D. Strand and A. Hoffmann for excellent technical assistance.

Author contributions
J.B., D.S. and M.M. designed research; B.K. performed HPLC analysis; S.G., V.F., K E.J, N.B. and L.S. performed research; A.K. and D.S. developed new reagents/tracer; S.L.K., T.B., T.B., T.W. and M.S. provided critical discussion; J.B., D.S. T.Bopp and M.M. wrote the paper.

Funding
Open Access funding enabled and organized by Projekt DEAL. This work was supported by the Deutsche Forschungsgemeinschaft (DFG), SFB 1292 TP01 (T.Bopp.), SFB 1066 project B13 (T.Bopp.), B8 (T.Bopp.) and B16N (T.Bopp., M.M. and T.W.), TR SFB 156 B11N (T.Bopp.),"Universitäres Centrum für Tumorerkrankungen (UCT)", and the "Forschungszentrum Immuntherapie (FZI)" of the University Medical Center.

Data availability
The datasets generated and/or analyzed during the current study are available from the corresponding author on reasonable request.

Declarations

Ethics approval and consent to participate
Animal experiments were approved by the Institutional Animal Care facility and by the competent governmental agency Landesuntersuchungsamt Rheinland-Pfalz (G 21–1-099). All animal procedures and methods were carried out in accordance with the approved guidelines and institutional regulations. Clinical trial number: not applicable.

Consent for publication
Not applicable.

Author details
[1]Department of Nuclear Medicine, University Medical Center Mainz, Mainz, Germany
[2]Max Planck Institute for Polymer Research Mainz, Mainz, Germany
[3]Department of Instructive Biomaterials Engineering, MERLN Institute for Technology-Inspired Regenerative Medicine, Maastricht University, Maastricht, The Netherlands
[4]Institute of Immunology, University Medical Center, Johannes Gutenberg University Mainz, Mainz, Germany
[5]Research Center for Immunotherapy (FZI), University Medical Center, Johannes Gutenberg University Mainz, Mainz, Germany
[6]University Cancer Center Mainz, University Medical Center, Johannes Gutenberg University Mainz, Mainz, Germany
[7]German Cancer Consortium (DKTK) Mainz, Mainz, Germany
[8]Department of Translational Imaging in Oncology, National Center for Tumor Diseases (NCT/UCC) Dresden, German Cancer Research Center (DKFZ) Heidelberg, and Helmholtz-Zentrum Dresden-Rossendorf (HZDR), Dresden, Germany
[9]Faculty of Medicine and University Hospital Carl Gustav Carus, University of Technology Dresden (TUD), German Cancer Research Center (DKFZ) Heidelberg, and Helmholtz-Zentrum Dresden-Rossendorf (HZDR), Dresden, Germany

Received: 5 March 2025 / Accepted: 22 January 2026
Published online: 05 February 2026

References

1. Boedtkjer E, Pedersen SF. The acidic tumor microenvironment as a driver of cancer. Annu Rev Physiol. 2020;82:103–26. https://doi.org/10.1146/annurev-physiol-021119-034627.
2. Barar J, Omidi Y. Dysregulated pH in tumor microenvironment checkmates cancer therapy. Bioimpacts. 2013;3:149–62. https://doi.org/10.5681/bi.2013.036.
3. Okreglak V, Ling R, Ingaramo M, Thayer NH, Millett-Sikking A, Gottschling DE. Cell cycle-linked vacuolar ph dynamics regulate amino acid homeostasis and cell growth. Nat Metab. 2023;5:1803–19. https://doi.org/10.1038/s42255-023-00872-1.
4. Wang JX, Choi SYC, Niu X, Kang N, Xue H, Killam J, et al. Lactic acid and an acidic tumor microenvironment suppress anticancer immunity. Int J Mol Sci. 2020. https://doi.org/10.3390/ijms21218363.
5. Wang ZH, Peng WB, Zhang P, Yang XP, Zhou Q. Lactate in the tumour microenvironment: from immune modulation to therapy. EBioMedicine. 2021;73:103627. https://doi.org/10.1016/j.ebiom.2021.103627.
6. Flavell RR, Truillet C, Regan MK, Ganguly T, Blecha JE, Kurhanewicz J, et al. Caged [(18)F]fdg glycosylamines for imaging acidic tumor microenvironments using positron emission tomography. Bioconjug Chem. 2016;27:170–8. https://doi.org/10.1021/acs.bioconjchem.5b00584.
7. Bohn T, Rapp S, Luther N, Klein M, Bruehl TJ, Kojima N, et al. Tumor immunoevasion via acidosis-dependent induction of regulatory tumor-associated macrophages. Nat Immunol. 2018;19:1319–29. https://doi.org/10.1038/s41590-018-0226-8.
8. Knopf P, Stowbur D, Hoffmann SHL, Hermann N, Maurer A, Bucher V, et al. Acidosis-mediated increase in IFN-γ-induced PD-L1 expression on cancer cells as an immune escape mechanism in solid tumors. Mol Cancer. 2023;22(1):207. https://doi.org/10.1186/s12943-023-01900-0.
9. Gallagher FA, Kettunen MI, Day SE, Hu DE, Ardenkjaer-Larsen JH, Zandt R, et al. Magnetic resonance imaging of pH in vivo using hyperpolarized 13C-labelled bicarbonate. Nature. 2008;453:940–3. https://doi.org/10.1038/nature07017.
10. Bauer D, Visca H, Weerakkody A, Carter LM, Samuels Z, Kaminsky S, et al. PET imaging of acidic tumor environment with (89)Zr-labeled pHLIP probes. Front Oncol. 2022;12:882541. https://doi.org/10.3389/fonc.2022.882541.
11. Demoin DW, Wyatt LC, Edwards KJ, Abdel-Atti D, Sarparanta M, Pourat J, et al. PET imaging of extracellular pH in tumors with (64)Cu- and (18)F-labeled pHLIP peptides: a structure-activity optimization study. Bioconjug Chem. 2016;27:2014–23. https://doi.org/10.1021/acs.bioconjchem.6b00306.
12. Isbell HS, Frush HL. Effect of para-H in the mutarotation and hydrolysis of glycosylamines. J Am Chem Soc. 1950;72:1043–4. https://doi.org/10.1021/ja01158a527.
13. Isbell HS, Frush HL. Mutarotation, hydrolysis, and rearrangement reactions of glycosylamines 1. J Org Chem. 1958;23:1309–19. https://doi.org/10.1021/jo01103a019.
14. Binauld S, Stenzel MH. Acid-degradable polymers for drug delivery: a decade of innovation. Chem Commun (Camb). 2013;49:2082–102. https://doi.org/10.1039/c2cc36589h.
15. Vaupel P, Schmidberger H, Mayer A. The warburg effect: essential part of metabolic reprogramming and central contributor to cancer progression. Int J Radiat Biol. 2019;95:912–9. https://doi.org/10.1080/09553002.2019.1589653.
16. Sun A, Tang X, Nie D, Fan Y, Tang G. Positron emission tomography imaging of lesions pH using (11)C-labeled bicarbonate. Cancer Biother Radiopharm. 2018;33:285–94. https://doi.org/10.1089/cbr.2017.2414.

17. Lau AZ, Miller JJ, Tyler DJ. Mapping of intracellular pH in the in vivo rodent heart using hyperpolarized [1-13C]pyruvate. Magn Reson Med. 2017;77:1810–7. https://doi.org/10.1002/mrm.26260.

Publisher's Note